

Probing the Global 21-cm Signal via the Integrated Sachs-Wolfe Effect on the 21-cm Background

Kyungjin Ahn* and Minji Oh

Department of Earth Sciences, Chosun University, Gwangju 61452, Korea

We propose a novel method to probe the global 21-cm background. This background experiences the integrated Sachs-Wolfe effect (ISW) as the cosmic microwave background does. The 21-cm ISW is modulated by the spectral shape of the global 21-cm signal, and thus the measure of the 21-cm ISW will be a probe of the evolution of the global signal. This strategy naturally mitigates the impact of the Milky Way foreground, which is a common and most significant challenge in conventional 21-cm background probes. With the phase-1 SKA telescope, probing the global 21-cm background would be feasible with a few 1000 hours of observation, enabling consistency checks with existing measures of the global 21-cm signal by EDGES and SARAS that are conflicting with each other.

I. INTRODUCTION

The anisotropy of the cosmic microwave background (CMB) is caused by various physical processes in the early and the late universe. Relatively weak yet detected with high significance is the late-time integrated Sachs-Wolfe effect [1] (ISW henceforth) on the CMB caused by the temporal variation of the large-scale gravitational potential in the relatively nearby universe [2–10]. In a Λ CDM universe, after the matter-dominated epoch, the gravitational potential changes in such a way that photons travel out of the potential well (bump) with less energy loss (gain) than the energy gain (loss) experienced while traveling into, causing the net blueshift (redshift) [1]. The measured ISW on CMB, originating from the last scattering surface at redshift $z \simeq 1000$, thus shows correlation with lower-redshift ($z \lesssim 2$) density tracers, or galaxies: the first proposal to use such a cross-correlation is by [11]. Aside from the possibility of the curvature density [12] or modified gravity effects [13, 14] for ISW, the measured ISW by galaxy-CMB correlation is consistent with the present-day dark energy content in units of the critical density at $\rho_\Lambda/\rho_{\text{crit},0} \sim 0.7$.

Redshifted 21-cm radiation from HI gas at $100 \gtrsim z \gtrsim 6$ is another radiation background that originates from high redshift and will experience the ISW effect. Its sky-averaged brightness temperature, or the global 21-cm background temperature ($\delta T_b(z)$ henceforth), has temporal variation determined by cosmology (baryon temperature and the collisional excitation of the spin-orbit angular momentum J of hydrogen) and astrophysics (impact on T from X-ray heating, the ultraviolet background due to early galaxies and the corresponding radiational excitation of J). Such a temporal evolution is marked by the observed frequency ν that is related to the originating redshift z through the relation $\nu = 1.42 \text{ GHz}/(1+z)$.

The main channel for the 21-cm background to be correlated with the low-redshift galaxies is through the

ISW effect (another subdominant channel in [5]). As will be shown in this paper, the temperature fluctuation of a frequency-dependent photon background caused by ISW is proportional to the amplitude of the global value and the spectral feedback:

$$\Delta T(\nu) \propto T(\nu) - \frac{\partial T(\nu)}{\partial \ln \nu}. \quad (1)$$

Therefore, one can in principle measure the cross-correlation between the 21-cm background in different frequency (redshift) bins and the galaxy distribution at low redshifts, and use the frequency variation in the cross-correlation to probe $\delta T_b(z)$.

The 21-cm ISW as a measurement of $\delta T_b(\nu) - \partial \delta T_b / \partial \ln \nu$ can then be used to check consistency with already existing observations of the global 21-cm signal by monoblock receivers: EDGES (Experiment to Detect the Global EoR Signature; [15]) and SARAS3 (Shaped Antenna measurement of the background Radio Spectrum, version 3; [16]). Both experiments measure the whole sky without interferometry, and a successful removal of the strong foreground composed of the Milky Way radio signal, the extragalactic background and CMB should be performed. These two experiments exhibit mutually conflicting results: the EDGES signal is reported to have $\delta T_b(\nu \sim 80 \text{ MHz}) \sim -500 \text{ mK}$, while the SARAS3 signal is consistent with a null result and rejects the EDGES signal at $\sim 1.8\sigma$. The absorption trough by the EDGES is much stronger than what is expected in the Λ CDM cosmology and thus has been interpreted as a possible signature for non-standard cosmology [17]. The refutation by SARAS3 seems justified as we have better control of its systematics than of the EDGES instrument [16]. However, the ambiguity in the foreground removal process is quite substantial in these “monopole-only” observations [18] and therefore an independent measurement of $\delta T_b(\nu)$ would be essential for confirmation. Our proposition here is one of such independent measurements.

Detecting the 21-cm ISW effect for the purpose of obtaining redundancy to the already-measured CMB ISW effect for cosmology has been proposed by [19].

* kjahn@chosun.ac.kr

We turn around their proposition and use the 21-cm ISW as a probe of $\delta T_b(z)$ using the dependence of the ISW on the global temperature (Eq. 1). We define an observable which is based on the 21-cm ISW and designed to probe $\delta T_b(\nu)$, different from what was used in [19]. This will be found practically equivalent to giving up the redundancy in cosmological information but instead gaining the information on the amplitude and the spectral shape of the global 21-cm background. We will show that such a probe would become practical with the upcoming Square Kilometre Array (SKA) aiming at the 21-cm background anisotropy from the $z \simeq 27 - 6$ universe, contrary to the pessimistic forecast by [19] who based the noise estimation at $z = 30$ which is too high for the sky noise to be controllable and used an observable different from what we will use in this paper.

The paper is organized as follows. In section II, we show how the 21-cm background is affected by ISW, and develop an observable based on the 21-cm ISW but aimed at probing $\delta T_b(z)$. In section III, we present estimated detectability of the observable with Phase-1 SKA specification to show its encouraging prospect. We also include the detectability when only using superstructures as 21-cm ISW drivers. In section IV, we discuss the observational strategy to realize the measurement and some caveat in our error estimates. Appendices are dedicated for technical details that were used for estimating observational uncertainties.

II. THEORY AND OBSERVABLE

A. Theory

We start from the energy equation of a photon on a line of sight of an observer, first calculated in [1]. All calculations henceforth are accurate to the linear order. A freely traveling photon reaching an observer at present experiences the temperature shift $\Delta T \equiv T - \langle T \rangle$ given by

$$\frac{\Delta T(\hat{n})}{\langle T \rangle} \Big|_{\eta_0} = \frac{\Delta T(\hat{n})}{\langle T \rangle} \Big|_{\eta_i} - \Psi(\eta_0) + \Psi(\eta_i) + \mathbf{v} \cdot \hat{n} \Big|_{\eta_i}^{\eta_0} + \int_{\eta_i}^{\eta_0} 2\Psi'(\hat{n}, \eta) d\eta, \quad (2)$$

where T is the temperature, $\langle T \rangle$ is the sky-averaged T (monopole), η_i and η_0 are the conformal times of some early onset (usually at CMB decoupling) and the present respectively, \hat{n} is the sky-direction unit vector, Ψ is the gravitational potential, and $' \equiv \partial/\partial\eta$. With η and Ψ , the Friedmann-Lemaître-Robertson-Walker metric perturbed in the linear order reads

$$ds^2 = a^2(\eta) \left\{ -(1 + 2\Psi)d\eta^2 + (1 - 2\Psi)\delta_{ij}dx^i dx^j \right\}, \quad (3)$$

where a is the scale factor, x^i is the comoving spatial coordinate, δ_{ij} is the Kronecker delta, and

only one perturbation term Ψ (as both the curvature perturbation and the gravitational potential) is sufficient when ignoring the anisotropic stress tensor (a valid approximation for the linear ISW: e.g. [3]). While taking η_i as the conformal time for the last scattering surface is usual in the CMB literature, we take $\eta_i \equiv \eta(z)$ to generalize for the background that originates from many different redshifts, such as the 21-cm background.

We now generalize Eq. (2) but focus only on the late-time ISW with a frequency-dependent brightness temperature¹ field (contrary to the CMB temperature which is independent of frequency). Also considering the global optical depth τ due to Thomson scattering by free electrons [7] for a collection of photons, we have

$$\frac{\Delta T(\nu, \hat{n})}{\langle T(\nu) \rangle} \Big|_{\eta_0} = \int_{\eta_i}^{\eta_0} e^{-\tau(\eta)} 2\Psi'(\hat{n}, \eta) d\eta \quad (4)$$

where $\tau(\eta) \equiv \int_{\eta}^{\eta_0} n_e(\eta) \sigma_T a(\eta) d\eta$, with the electron number density n_e , the scale factor a and the Thomson scattering cross section σ_T . In practice, in the Λ CDM framework, ISW becomes effective only after $\Omega_\Lambda \sim \Omega_m$ (or at $z \lesssim 2$) and thus the exact value of η_i does not matter. The observed frequency, excluding the kinematically induced dipole [20], is shifted from the cosmological one as ²

$$\nu(\hat{n}, z) - \bar{\nu}(z) = \int_{\eta_i}^{\eta_0} 2\Psi' d\eta \quad (5)$$

where $\bar{\nu}(z) \equiv \nu_{21}/(1+z) = 1420 \text{ MHz}/(1+z)$, whose z -dependence will henceforth be dropped in notation for simplicity, is the redshifted 21-cm line frequency in an unperturbed universe. As shown in [19], combining Eqs. (4) and (5), the observed temperature difference at $\bar{\nu}$ becomes

$$\begin{aligned} \Delta T(\bar{\nu}, \hat{n}) &= \langle T(\bar{\nu}) \rangle \int_{\eta_i}^{\eta_0} \left(e^{-\tau(\eta)} - \frac{\partial \ln \langle T(\bar{\nu}) \rangle}{\partial \ln \bar{\nu}} \right) 2\Psi'(\hat{n}, \eta) d\eta \\ &\simeq \left(\langle T(\bar{\nu}) \rangle - \frac{\partial \langle T(\bar{\nu}) \rangle}{\partial \ln \bar{\nu}} \right) \int_{\eta_i}^{\eta_0} 2\Psi'(\hat{n}, \eta) d\eta, \end{aligned} \quad (6)$$

where the spectral feedback term including $\partial \langle T(\bar{\nu}) \rangle / \partial \ln \bar{\nu}$ arises when we Taylor-expand $\Delta T(\nu, \hat{n})$ into terms in $\bar{\nu}$, with the help of Eq. (5). Physically, this feedback occurs because, when an ISW driver (e.g. a potential well) shifts the observed frequency and temperature, the observer probes the temperature

¹ One could instead formulate the 21-cm ISW in terms of the flux density or the specific intensity, whose amplitude at frequency ν (redshift z for spectral-line backgrounds) defines the brightness temperature $T(\nu)$ ($T(z)$) that needs not be a thermal temperature, in general, as in the case of the 21-cm brightness temperature.

² Note the disappearance of $\exp[-\tau(\eta)]$ term compared to Eq. (4).

fluctuation situated at the other frequency modulated by the same ISW effect. In comparison, the CMB-only shift becomes (we denote the CMB by “ γ ” throughout this paper)

$$\begin{aligned}\Delta T_{\gamma,0}(\hat{n}) &= \langle T_{\gamma,0} \rangle \int_{\eta_i}^{\eta_0} e^{-\tau(\eta)} 2\Psi'(\hat{n}, \eta) d\eta \\ &\simeq \langle T_{\gamma,0} \rangle \int_{\eta_i}^{\eta_0} 2\Psi'(\hat{n}, \eta) d\eta.\end{aligned}\quad (7)$$

In Eqs. (6) and (7), we approximated $\tau(\eta) \simeq 0$ because only the late, low-density universe obtains the optical depth in the case of ISW. In the concurrent Λ CDM model, the ISW-relevant (when $\Psi' \neq 0$) regime limits $\tau(\eta) \lesssim \tau(z \leq 2) \simeq 0.0087$, and thus this approximation is justified if one were not to calculate the ISW effect at sub-percent level accuracy.

The low-frequency global temperature is the one shifted from the global CMB temperature $\langle T_{\gamma,0} \rangle$ ($= 2.725$ K) such that $\langle T(\bar{\nu}) \rangle = \langle T_{\gamma,0} \rangle + \delta T_b(\bar{\nu}) + T_{\text{FG}}(\bar{\nu})$, where $\delta T_b(\bar{\nu})$ is the global 21-cm brightness temperature and $T_{\text{FG}}(\bar{\nu})$ is the foreground temperature by the Milky Way, extragalaxies, and possibly some unknown foreground (background). Let us assume for the sake of discussion that T_{FG} comes mostly from the Milky Way and thus does not produce any ISW effect. This will be realized by correlating the temperature field with the galaxy distribution. Then, one can readily see that the ISW effect on the low-frequency temperature deviates from that of the CMB according to

$$\Delta T(\bar{\nu}, \hat{n}) = \Delta T_{\gamma,0}(\hat{n}) \left(1 + \frac{\delta T_{21}(\bar{\nu})}{\langle T_{\gamma,0} \rangle} \right), \quad (8)$$

where

$$\delta T_{21}(\bar{\nu}) \equiv \delta T_b(\bar{\nu}) - \frac{\partial \delta T_b(\bar{\nu})}{\partial \ln \bar{\nu}}. \quad (9)$$

Therefore, measuring the low-frequency ISW effect at varying frequencies and comparing this to the CMB ISW will enable one to probe $\delta T_b(\bar{\nu})$ or more directly $\delta T_{21}(\bar{\nu})$.

The galaxy-temperature cross-correlation has been the only practical measure of the ISW for CMB, and it will be much more so for the 21-cm due to the weakness of the signal. The cross-correlation angular power spectrum of $\Delta T(\bar{\nu}, \hat{n})$ in the radio frequency and galaxy overdensity δ_g at observing frequency $\bar{\nu}$ is given by

$$\begin{aligned}C_\ell^{gT}(\bar{\nu}) &= \{ \langle T_{\gamma,0} \rangle + \delta T_{21}(\bar{\nu}) \} \\ &4\pi \int d \ln k \Delta_0^2(k) W_\ell^g(k) W_\ell^{\text{ISW}}(k),\end{aligned}\quad (10)$$

which is a specific case of the general correlation angular power spectrum of fields X and Y (see Appendix A for details),

$$C_\ell^{XY}(\bar{\nu}) = N^{XY}(\bar{\nu}) 4\pi \int d \ln k \Delta_0^2(k) W_\ell^X(k) W_\ell^Y(k), \quad (11)$$

with $X = g$, $Y = T$ and $N^{gT}(\bar{\nu}) = \langle T_{\gamma,0} \rangle + \delta T_{21}(\bar{\nu})$. In equations (10) and (11), $W_\ell^X(k)$ is the window function for a field X relating the wavenumber k of the field to the multipole ℓ projected on the sky. $\Delta_0^2(k) \equiv k^3 P_0(k)/2\pi^2$ is the variance of the present-day matter power spectrum $P_0(k)$,

$$\begin{aligned}W_\ell^g(k) &= \int dz b(z) \phi(z) D(z) j_\ell[kr(z)], \\ W_\ell^{\text{ISW}}(k) &= \int dz \frac{3\Omega_{m,0} H_0^2}{k^2} \frac{dg}{dz} j_\ell[kr(z)],\end{aligned}\quad (12)$$

$\phi(z)$ is the normalized galaxy selection function [7], $b(z)$ is the linear galaxy bias, $D(z)$ is the linear growth factor of the density fluctuation, j_ℓ is the spherical Bessel function of order ℓ , $r(z) = \eta_0 - \eta(z)$ is the comoving distance, $\Omega_{m,0}$ is the matter fraction at present, H_0 is the Hubble parameter at present, and $g(z) = D(z)(1+z)$ is the linear growth factor of the gravitational potential³. If the foreground comes only from the nearby ($z \simeq 0$) universe, $C_\ell^{gT_{\text{FG}}} = 0$ and thus $C_\ell^{gT}(\bar{\nu}) \propto (\langle T_{\gamma,0} \rangle + \delta T_{21}(\bar{\nu}))$ as we put in Eq. (12). However, some fraction of the foreground can originate from higher redshift range, which is the subject we discuss in Section IV.

B. Observable

We define an observable as a combination of $C_\ell^{gT}(\bar{\nu})$ and $C_\ell^{gT_\gamma}$. In principle, both quantities will have the identical angular pattern on the sky, because ISWs on the CMB and the 21-cm background are caused by the same gravitational potentials that are probed by galaxies. This enables an observable which converges to a single scalar quantity for any multipole ℓ , as will be shown in the following. The key forecast will be presented in Fig. 1 and Section III A.

A special, frequency-independent version of Eq. (10) with $\delta T_{21} = 0$ is the usual high-frequency CMB one, $C_\ell^{gT_\gamma}$. It is obvious that we can extract the global 21-cm signal by defining

$$s_\ell(\bar{\nu}) \equiv \langle T_{\gamma,0} \rangle \left(\frac{C_\ell^{gT}(\bar{\nu})}{C_\ell^{gT_\gamma}} - 1 \right) = \delta T_{21}(\bar{\nu}). \quad (13)$$

Note that $s_\ell(\bar{\nu})$ turns out to be independent of ℓ . The cumulative signal

$$S(\bar{\nu}) \equiv \frac{\sum_{\ell=\ell_{\min}}^{\ell_{\max}} s_\ell(\bar{\nu})}{(\ell_{\max} - \ell_{\min} + 1)} = \delta T_{21}(\bar{\nu}) \quad (14)$$

will maximize the net sensitivity with many harmonics, where we take $\ell_{\min} = 2$ and $\ell_{\max} = 100$. In practice,

³ For a pedagogical derivation of the ISW cross power, see Ref. [3, 21], which yields Eq. (12).

$\ell_{\max} \sim 20$ is already large enough to saturate SNR of

$S(\bar{\nu})$, as will be seen in Fig. 2. The cumulative SNR for $S(\bar{\nu})$ is given by⁴ (derivation given in Appendix B 1)

$$\left(\frac{S}{N}\right)^2(\bar{\nu}) = \sum_{\ell=\ell_{\min}}^{\ell_{\max}} \left(\frac{\delta T_{21}(\bar{\nu})}{\sigma_{s_\ell}(\bar{\nu})}\right)^2 = \frac{\delta T_{21}^2(\bar{\nu})}{\langle T_{\gamma,0} \rangle^2} \sum_{\ell=\ell_{\min}}^{\ell_{\max}} \left[\frac{(C_\ell^{gg} + \bar{n}_g^{-1}) \left\{ C_\ell^{\delta T_b \delta T_b}(\bar{\nu}) + \epsilon_{\ell,T}(\bar{\nu}) + \left(\frac{\delta T_{21}(\bar{\nu})}{\langle T_{\gamma,0} \rangle}\right)^2 C_\ell^{T_\gamma T_\gamma} \right\}}{(C_\ell^{gT_\gamma})^2 f_{\text{sky}}(2\ell+1)} \right]^{-1}, \quad (15)$$

where f_{sky} is the sky coverage, \bar{n}_g is the surface number density of ISW galaxies (total number of galaxies per steradian), $\epsilon_{\ell,T}$ is the 21-cm systematic error due to the sky brightness given as

$$\epsilon_{\ell,T} = \frac{2\pi\lambda^2(\bar{\nu}) \left\{ 180(\bar{\nu}/180 \text{ MHz})^{-2.6} \text{ K} \right\}^2}{f_{\text{cov}}^2 D^2 \Delta t \Delta \nu} \quad (16)$$

with the observing wavelength λ , the maximum baseline D of the densely spaced core of interferometers, the observing time Δt , the land coverage f_{cov} , and the bandwidth $\Delta \nu$ [22]. We have normalization coefficients (Eq. 11) $N_\ell^{\delta T_b \delta T_b} = \delta T_b^2(\bar{\nu})$, $N_\ell^{gT_\gamma} = T_{\gamma,0}$ and $N_\ell^{T_\gamma T_\gamma} = T_{\gamma,0}^2$. Especially, $C_\ell^{\delta T_b \delta T_b}$ is dominated by the primordial power spectrum with negligible contribution from the auto-correlation of the 21-cm ISW (Appendix B 1), and thus the net power $C_\ell^{\delta T_b \delta T_b}$ does not get boosted by the spectral feedback term $\partial \delta T_b(\bar{\nu}) / \partial \ln \bar{\nu}$. This is an important fact that renders the noise controllable during the epoch when the noise is dominated not by $\epsilon_{\ell,T}$ but by $C_\ell^{\delta T_b \delta T_b}(\bar{\nu})$. The noise on $s_\ell(\bar{\nu})$, or $\sigma_{s_\ell}(\bar{\nu})$, depends on the spectral shape of $\delta T_b(\bar{\nu})$ and thus SNR depends on cosmology and astrophysics. Note that one should also consider the noise $\sigma_{\langle T_{\gamma,0} \rangle}$ in the global CMB temperature due to our definition of the signal (Eq. 13); however, we find it negligible already with the FIRAS observation giving $\sigma_{\langle T_{\gamma,0} \rangle} = 0.57 \text{ mK}$ [23, 24] while the net noise $S(\bar{\nu})/(S/N)(\bar{\nu})$ hardly reaches such a small value, and always residing at $> 20 \text{ mK}$ with all the observational configurations considered in this paper.

III. RESULT

A. full-sky observation

We test three distinctive 21-cm models and estimate $(S/N)(\bar{\nu})$ given in Eq. (15). We consider two different

strategies in measuring C_ℓ^{gT} : (1) the usual full-sky ISW measurement and (2) the ISW measurement only through superstructures [8, 25–31], to be described in Section III B. The test models are (1) “V” (vanilla), a typical Λ CDM model with galaxies without much feedback on their formation [32], (2) “SR II” (self-regulated type II), a model under the Λ CDM framework but with strong self-regulation of galaxy formation during the cosmic dawn [33, 34], and (3) “NS” (non-standard): a model beyond Λ CDM that has a large dip of $\delta T_b \simeq -500 \text{ mK}$ around $\nu \simeq 80 \text{ MHz}$, having resemblance to the EDGES signal. All these models have $\delta T_b > 0$ at $z \lesssim 9$ with steep upturns at higher frequencies, which is believed to be natural with moderate X-ray heating and consistent with what is indicated by the upper limits on the 21-cm fluctuation put by some of the SKA precursors [35–37]. Therefore, all these models have epochs with steep slopes in $\delta T_b(\bar{\nu})$ such that $|\partial \delta T_b / \partial \ln \bar{\nu}| \simeq [2 - 8] |\delta T_b|$ in some range of frequencies and the net signal δT_{21} can be greatly amplified from δT_b .

We take the following observational parameters that are suitable with the $\sim 1\text{-km}$ core region of the Square Kilometre Array: $D = 1 \text{ km}$, $f_{\text{cov}} = 0.25$, $\Delta t = \{3000, 10000, 30000\} \text{ hr}$, $f_{\text{sky}} = 0.7$, $\Delta \nu = 5 \text{ MHz}$, and galaxy surveys satisfying: $\bar{n}_g \geq (b/2)^{-2} \times 10^7 \text{ sr}^{-1}$ where $b \equiv \langle b(z) \rangle$ is the average galaxy bias. The last condition and the large f_{sky} requirement are already met with the Wide-Field Infrared Survey Explorer (WISE) galaxy catalogues [8, 38], and will get more surpassed by the upcoming full-sky galaxy survey Spectro-Photometer for the History of the Universe, Epoch of Reionization, and Ices Explorer (SPHEREx) [39]. We find that uncertainty due to the galaxy shot noise starts to take effect, mostly at $\bar{\nu} \gtrsim 160 \text{ MHz}$, when \bar{n}_g fails to satisfy the above criterion.

The prospect of using the observable $S(\bar{\nu})$ as a probe of the global 21-cm signal is encouraging (Fig. 1). Due to the non-existence of the correlation between the Milky Way (dominating the radio sky) and the 21-cm background, our method is free from the ambiguity in the foreground removal⁵. Except for the dark ages ($z \gtrsim 30$; $\bar{\nu}/\text{MHz} \lesssim 46$), we can achieve reasonably

⁴ This is a rough estimate; a more accurate error estimate should be taken for the effect of the masking at least. In practice, $C_\ell^{T_\gamma T_\gamma}$ measured by the Planck telescope is limited only by cosmic variance at $\ell \lesssim 1100$, and thus we may neglect the detector noise in Eq. (15).

⁵ The impact by extragalactic and unknown foregrounds still exist, which is addressed in Section IV.

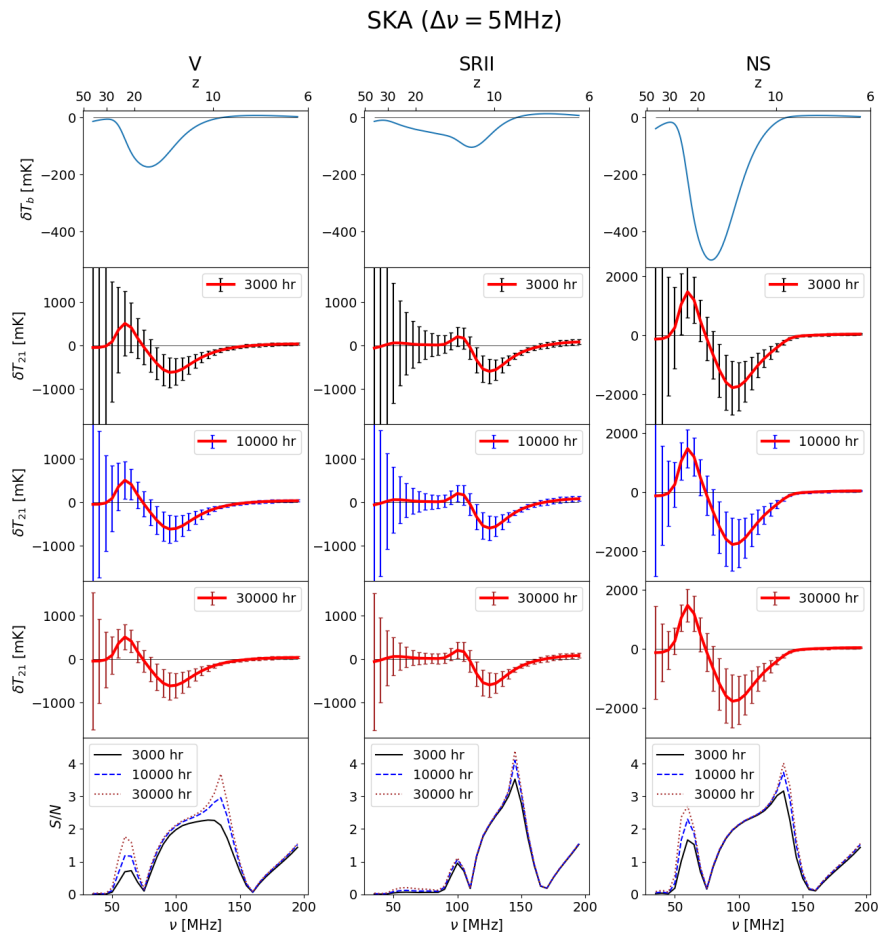


FIG. 1. Forecasts for measuring the global 21-cm background $\delta T_{21}(\nu) = \delta T_b(\nu) - \partial \delta T_b / \partial \ln \nu$, through observing the 21-cm ISW effect by the SKA1-LOW telescope with 3000-, 10000- and 30000-hour observing times and 5-MHz bandwidth on 70% of the sky. Mock signals from three different test models (V: left, SRII: middle, NS: right) are used. From top to bottom, subpanels show the spectra of δT_b (top), spectra of the observable (thick, red), δT_{21} , with $1\text{-}\sigma$ error bars when $\Delta t=3000$ (2nd from top), 10000 (middle) and 30000 (4th from top) hours, and finally SNRs (bottom). Error bars and SNR curves follow the same line-color convention (3000 hr: black; 10000 hr: blue; 30000 hr: brown). While there is model dependency, moderate to high-significance detection of δT_{21} , and thus δT_b , from the cosmic dawn and the epoch of reionization is feasible, with the exception for the shallow-slope (in δT_b) case of SRII at $z \gtrsim 13$ ($\nu \lesssim 100$ MHz). Observation during the dark ages ($z \gtrsim 30$) remains impossible with our strategy in all cases, due to the ever increasing sky brightness as frequency decreases.

high SNR in probing both the cosmic dawn ($15 \lesssim z \lesssim 30$; $89 \gtrsim \bar{\nu}/\text{MHz} \gtrsim 46$) and the epoch of reionization ($6 \lesssim z \lesssim 15$; $202 \gtrsim \bar{\nu}/\text{MHz} \gtrsim 89$) only with the exception of SRII having low SNR in the cosmic dawn. Especially, the NS case has $\gtrsim (2-3)\sigma$ detectability per frequency band, and thus the 21-cm ISW observation would either rule out or detect the non-standard universe with relatively high significance (compared to the expected theoretical maximum SNR for CMB ISW [3, 11], $\text{SNR} \sim 7-9$, this can be considered high significance). The 21-cm ISW observation would thus place a significant constraint on the global 21-cm background, and allow consistency checks with the previous, mutually conflicting observations of $\delta T_b(\bar{\nu})$ by the EDGES and the SARAS.

B. superstructure observation

Can we use the superstructures (superclusters and supervoids) as the 21-cm ISW driver and probe the global 21-cm background? We find that such a strategy is impractical even with planned telescopes at the moment. The superstructure ISW effect on CMB has been found to be about $A_{\text{ISW}} \simeq 1.5 - 5$, where A_{ISW} is the ratio of the observed ΔT in superstructures to the ΔT expected in ΛCDM due to ISW. Recent analyses such as [28, 30] with carefully chosen convolution filters, which are used to identify and characterize superstructures, find that ISW in these regions is only marginally amplified, or $A_{\text{ISW}} \sim 1.5$, and thus consistent with ΛCDM . Analyses beforehand using a rather special convolution filter used to find $A_{\text{ISW}} \sim 5$, too large to be due to

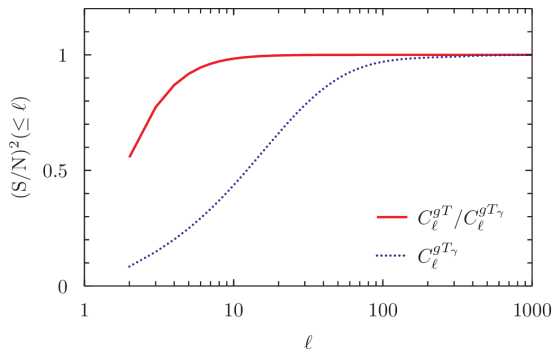


FIG. 2. Cumulative $(S/N)^2(\leq \ell) \equiv \sum_{\ell'=2}^{\ell} (S/N)^2(\ell')$ for the 21-cm probe $S(\bar{\nu})$ at a representative frequency $\bar{\nu} = 90$ MHz (red, solid) and for the CMB-ISW cross-correlation $C_{\ell}^{gT_{\gamma}}$ (blue, dotted). Curves are normalized to show relative importance of modes for the two cases, such that the saturated $(S/N)^2$ reaches 1 in both cases. Most of the contribution comes from modes at $\ell \lesssim 20$ in the 21-cm probe, while from modes at $\ell \lesssim 200$ in the CMB-ISW cross-correlation. Therefore, it is necessary to accurately probe the largest scales of the sky for the 21-cm-ISW correlation, and also for the CMB-ISW correlation because the net observable is the combination of the two cross-correlations.

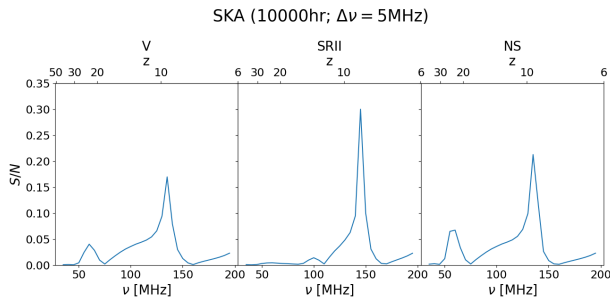


FIG. 3. Forecasts for measuring the global 21-cm background $\delta T_{21}(\nu)$ via stacked 21-cm ISW effect on ~ 200 superclusters, with $\Delta\nu = 5$ MHz and observing time of 10000 hours by SKA. In all the tested cases with SKA, SNRs are too low for such observations to be practical, leaving the full-sky observation (Fig. 1) the only viable strategy.

the ISW in Λ CDM [8, 25–27, 29, 31]. Whether or not the superstructure ISW is consistent with the standard cosmology, we may use these as the 21-cm ISW drivers.

The 21-cm ISW by superstructures will have

$$\Delta T^{\text{ISW}}(\bar{\nu}) = A_{\text{ISW}} \frac{\delta T_{21}(\bar{\nu})}{T_{\gamma,0}} \Delta \tilde{T}_{\gamma}^{\text{ISW}}, \quad (17)$$

with the theoretically expected $\Delta \tilde{T}_{\gamma}^{\text{ISW}} \simeq 2 \mu\text{K}$ on superstructures in Λ CDM [25, 28] and comparing this signal to the expected noise inside superstructures, we obtain SNR which is well below 1 in the full frequency range (Fig. 3; calculation of SNR described in Appendix B2). This is so even when we use $A_{\text{ISW}} = 5$. Note that the signal is the average of the stacked $\Delta T^{\text{ISW}}(\bar{\nu})$, where we assumed stacking of 200

superstructures that is comparable to the number of superstructures used in [25, 26] to reduce the noise in measuring the CMB ISW.

IV. DISCUSSION

We briefly remark on the impact of the extragalactic foreground and some possible unknown foreground. As stressed earlier, we have null contribution from any radiation of the Milky Way origin, or $C_{\ell}^{gT^{\text{MW}}}(\bar{\nu}) = 0$. Even so, foregrounds of other origin can be problematic. First, extragalactic foreground can be correlated with the late-time galaxy distribution simply because radio emission from these galaxies exist. Therefore,

$$C_{\ell}^{gT}(\bar{\nu}) = C_{\ell}^{gT^{\text{exgal}}}(\bar{\nu}) + C_{\ell}^{gT^{\text{unknown}}}(\bar{\nu}) + C_{\ell}^{g\delta T_b}(\bar{\nu}) \quad (18)$$

in general. Further, both these foregrounds can be decomposed into the intrinsic and ISW-driven parts, because if a part of radiation comes from high redshift, $z \gtrsim 2$, that part of the foreground can also experience the ISW by galaxies at $z \lesssim 2$. The same logic will apply to some unknown foreground. Therefore, in practice, removal of extragalactic and unknown foregrounds from the field of $C_{\ell}^{gT}(\bar{\nu})$ will still be necessary. We will further investigate this issue in a future study.

According to what is shown in Section III, we conclude that the full-sky 21-cm ISW measurement by radio interferometers is the only practical way to probe the global 21-cm background through ISW. Observing the kinematically induced multipole moments of the 21-cm background anisotropy due to the motion of the earth is another independent measure of the global 21-cm background as we suggested elsewhere [20, 40]. There are pros and cons of these two observational strategies, which are complementary to each other. The 21-cm ISW observation does not suffer from the imperfect removal of the Milky Way foreground, thanks to the null cross-correlation with the 21-cm background, while requires interferometric telescopes still in the future with very high sensitivity, such as SKA and HERA. The multipole (practically dipole and possibly quadrupole at best) observation requires much smaller telescopes, while the foreground removal process in each multipole is still required.

For observation of the 21-cm ISW, both HERA (with a strong limitation described below though) and SKA1-LOW (phase-1 SKA in low frequency) meet the thermal noise requirement. However, SKA1-LOW will be the only choice at the moment. HERA is a telescope with $D = 300$ m and $f_{\text{cov}} \simeq 0.75$ for the collecting area in the core region to reach 51000 m^2 . This is roughly the same as what we assumed in this paper for SKA in terms of Df_{cov} , but the 21-cm ISW observation with HERA would become practical only if the full-sky observation can be performed with the addition of the beam-forming capability. This is because the largest-scale modes should be probed and also the sky coverage

is essential to achieve high SNR (Eq. 15). Currently, HERA is planned to observe 1440-deg² sky which is far too small for the ISW observation. The core region of SKA1-LOW is what we have assumed as the SKA-core configuration in this paper, planned to be spread over the circular area of $D \simeq 1$ km with the total collecting area ~ 215000 m², or $f_{\text{cov}} \simeq 0.27$. We even find that 3000-hr integration would still give moderate SNR at $\nu \gtrsim 90$ MHz. Therefore, the predicted SNR of this paper will become possible with $\gtrsim 1$ -year operation of SKA1-LOW, which practically amounts to about $\gtrsim 2000$ – 4000 -hr observation time depending on the observing condition throughout the total observing time Δt . With the expected completion of SKA1-LOW construction in year 2029, probing the global 21-cm background through the 21-cm ISW observation could be realized within about a decade from now.

We note that the currently planned observational strategy for SKA1-LOW is likely to be unsuitable for the full-sky 21-cm ISW observation we propose here. The survey area on the sky for SKA1-LOW 21-cm background observation is expected to be limited, to gain very high sensitivity for scales of common interest in the EoR science: $k \sim 0.1$ – 1 Mpc⁻¹ [41]. However, our proposal is quite promising in terms of both sensitivity and mitigated foreground effect (that of the Milky Way especially). Therefore, we suggest that our proposal for the low-angular-resolution, full-sky ($\ell \lesssim 20$) observation be given serious consideration as a new science potential of the SKA.

ACKNOWLEDGMENTS

KA is supported by NRF-2021R1A2C1095136 and a research grant from Chosun University (2018).

Appendix A: angular power spectrum of auto- and cross-correlation

For theoretical estimates of the signals and noises, the angular power spectra of the auto- and cross-correlation are required. The angular power spectrum of the cross-correlation between fields X and Y is given by

$$C_{\ell}^{XY}(\bar{\nu}) = N^{XY}(\bar{\nu}) 4\pi \int d \ln k \Delta_0^2(k) W_{\ell}^X(k) W_{\ell}^Y(k), \quad (\text{A1})$$

where N^{XY} is the coefficient that renders C_{ℓ}^{XY} to be dimensional when a temperature field is involved, and the frequency dependence in C_{ℓ}^{XY} and N^{XY} appears when the 21-cm background is involved. Window functions $W_{\ell}(k)$ are shown in Eq. (12) of the main text. This dimensional definition of C_{ℓ}^{XY} is convenient as we use two different temperature fields (CMB and 21-cm background), and the 21-cm background experiences the spectral feedback by the ISW while the CMB does not.

Eq. (A1) can be applied for the auto-correlation of the galaxy overdensity, and of the ISW-affected temperature fields. N^{XY} 's are given by

$$N^{gg} = 1; \quad N^{gT_{\gamma}} = T_{\gamma,0}; \quad N^{g\delta T_b}(\bar{\nu}) = \delta T_{21}(\bar{\nu}). \quad (\text{A2})$$

In both backgrounds, the temperature autocorrelations $C_{\ell}^{T_{\gamma}T_{\gamma}}$ and $C_{\ell}^{\delta T_b\delta T_b}$ are dominated by the primordial fluctuations, not by the ISW-driven fluctuations [7]. We obtain $C_{\ell}^{T_{\gamma}T_{\gamma}}$ using the Boltzmann solver ‘‘Code for Anisotropies in the Microwave Background’’ (CAMB; [42]). With a reasonable assumption of linearity, we can still use Eq. (A1) to obtain $C_{\ell}^{\delta T_b\delta T_b}(\bar{\nu})$ using the matter density fluctuation:

$$N_{\ell}^{\delta T_b\delta T_b}(\bar{\nu}) = \delta^2 T_b(\bar{\nu}),$$

$$W_{\ell}^{\delta T_b}(\bar{\nu}) = \int^{\Delta z(\bar{\nu})} dz D(z) j_{\ell}[kr(z)] / \Delta z(\bar{\nu}), \quad (\text{A3})$$

where $\Delta z(\bar{\nu})$ is the redshift range defined by the given frequency bandwidth around $\bar{\nu}$, and in effect W_{ℓ}^g (Eq. 12) is used with $\phi(z) = 1/\Delta z$ and $b(z) = 1$. Because at high redshift, very small wavenumbers $k \sim (\ell + 1/2)/r(z = 30-6) \lesssim 0.002$ – 0.003 h Mpc⁻¹ become relevant in the range of harmonics relevant to the 21-cm ISW, $\ell \lesssim 20$ (see Fig. 2), and thus the nonlinear effects from the photon-intensity fluctuations and the inhomogeneous H II structure do not count much in calculating $C_{\ell}^{\delta T_b\delta T_b}(\bar{\nu})$ [43]. As stressed in the main text, it is important to notice that $N_{\ell}^{\delta T_b\delta T_b}(\bar{\nu})$ is equal not to $\delta^2 T_{21}(\bar{\nu})$ but to $\delta^2 T_b(\bar{\nu})$, because otherwise the noise would have been uncontrollably large.

We use $b(z) = 2$ and a smooth selection function [7]

$$\phi(z) = \frac{1}{\Gamma\left(\frac{\alpha+1}{\beta}\right)} \beta \frac{z^{\alpha}}{z_0^{\alpha+1}} \exp\left[-\left(\frac{z}{z_0}\right)^{\beta}\right] \quad (\text{A4})$$

with $\alpha = 3.457$, $\beta = 1.1$, $z_0 = 0.3$, peaking at $z \simeq 0.8$. We experimented with different values of $\{\alpha, \beta, z_0\}$ and find that our error estimation is hardly affected by these quantities. The dependence on $b(z)$ roughly appears as the limit we find, $\bar{n}_g \geq (b/2)^{-2} 10^7$ sr⁻¹, that saturates the SNR at the maximum values we find for values of $\{\alpha, \beta, z_0\}$ above (Fig. 1 in the main text). Note that the observable $S(\bar{\nu})$ is hardly affected by $b(z)$, because its dependence cancels out when the division $C_{\ell}^{gT}(\bar{\nu})/C_{\ell}^{gT_{\gamma}}$ is made. This limit on \bar{n}_g might be relaxed if $\phi(z)$ were peaked at lower redshifts than we have chosen here, due to the relative increase in C_{ℓ}^{gg} . We have calculated the integration in W_{ℓ}^X 's by using the ‘‘FFTLog’’ algorithm developed elsewhere [44], instead of using the Limber approximation. Fig. 4 shows dimensionless auto- and cross-correlations C_{ℓ}^{XY}/N^{XY} we obtained.

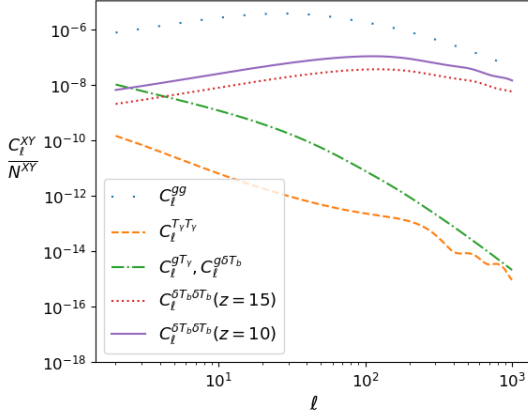


FIG. 4. Dimensionless auto- and cross-correlation power spectrum of the galaxy (“g”), the CMB temperature (“ T_γ ”) and the 21-cm temperature (“ δT_b ”).

Appendix B: Noise in observables

1. full-sky 21-cm ISW

The observable $s_\ell(\bar{\nu})$ defined in Eq. (13) of the main text has the noise spectrum $\sigma_{s_\ell}(\bar{\nu})$ to be shown in Eq.

(B8) below. We show how we obtained the expression. First, one should start from the error propagation (we drop the frequency dependence for readability):

$$\sigma_{s_\ell}^2 = T_{\gamma,0}^2 \left(\frac{C_\ell^{gT}}{C_\ell^{gT_\gamma}} \right)^2 \left(\frac{\sigma_{C_\ell^{gT}}^2}{(C_\ell^{gT})^2} + \frac{\sigma_{C_\ell^{gT_\gamma}}^2}{(C_\ell^{gT_\gamma})^2} - 2 \frac{\sigma_{C_\ell^{gT} C_\ell^{gT_\gamma}}}{C_\ell^{gT} C_\ell^{gT_\gamma}} \right), \quad (\text{B1})$$

where we ignored the variance in the global CMB temperature $\sigma_{T_{\gamma,0}}^2 = 0.57^2 \text{ mK}^2$, which is much smaller than the net noise we find (see Fig. 5). Realizing mutually related gaussian fields at given harmonics (ℓ , m) by combinations of independent gaussian fields are useful [45, 46]:

$$\begin{aligned} a_{\ell m}^g &= \sqrt{C_\ell^{gg}} \psi_{1,\ell m}, \\ a_{\ell m}^{T_\gamma} &= \frac{C_\ell^{gT_\gamma}}{\sqrt{C_\ell^{gg}}} \psi_{1,\ell m} + \sqrt{C_\ell^{T_\gamma T_\gamma} - \frac{(C_\ell^{gT_\gamma})^2}{C_\ell^{gg}}} \psi_{2,\ell m}, \\ a_{\ell m}^T &= \frac{C_\ell^{gT}}{\sqrt{C_\ell^{gg}}} \psi_{1,\ell m} + \left(C_\ell^{T_\gamma T} - \frac{C_\ell^{gT_\gamma} C_\ell^{gT}}{C_\ell^{gg}} \right) / \sqrt{C_\ell^{T_\gamma T_\gamma} - \frac{(C_\ell^{gT_\gamma})^2}{C_\ell^{gg}}} \psi_{2,\ell m} \\ &\quad + \sqrt{C_\ell^{TT} - \frac{C_\ell^{T_\gamma T_\gamma} (C_\ell^{gT})^2 + C_\ell^{gg} (C_\ell^{T_\gamma T})^2 - 2 C_\ell^{gT_\gamma} C_\ell^{gT} C_\ell^{T_\gamma T}}{C_\ell^{gg} C_\ell^{T_\gamma T_\gamma} - (C_\ell^{gT_\gamma})^2}} \psi_{3,\ell m}, \end{aligned} \quad (\text{B2})$$

where $\psi_{1,\ell m}$, $\psi_{2,\ell m}$, and $\psi_{3,\ell m}$ are mutually independent, unit-variance gaussian random fields for harmonics (ℓ , m) that satisfy

$$\begin{aligned} \langle \psi_{i,\ell m} \psi_{j,\ell m} \rangle &= \delta_{ij}, \\ \langle \psi_{i,\ell m}^3 \psi_{j,\ell m} \rangle &= 3\delta_{ij}, \\ \langle \psi_{i,\ell m}^2 \psi_{j,\ell m}^2 \rangle &= 3\delta_{ij} + (1 - \delta_{ij}), \end{aligned} \quad (\text{B3})$$

where $\langle \rangle$ denotes the ensemble average. We also use the fact

$$\begin{aligned} C_\ell^{gT} &= C_\ell^{gT_\gamma} + C_\ell^{\delta T_b} = \left(1 + \frac{\delta T_{21}}{T_{\gamma,0}} \right) C_\ell^{gT_\gamma}, \\ C_\ell^{TT} &= C_\ell^{T_\gamma T_\gamma} + C_\ell^{\delta T_b \delta T_b}, \\ C_\ell^{T_\gamma T} &= C_\ell^{T_\gamma T_\gamma}, \end{aligned} \quad (\text{B4})$$

where we assumed $C_\ell^{T_\gamma \delta T_b} = 0$ in the last two equations, which is just an approximation because the evolving Doppler effect during reionization can give a substantial cross-correlation between the 21-cm background and CMB, especially so when reionization proceeds fast, yet

still subdominant to $C_\ell^{T_\gamma T_\gamma}$ [47]. Also another cross-correlation comes through the common ISW effect:

$$C_\ell^{T_\gamma \delta T_b} = \frac{C_\ell^{g T_\gamma} C_\ell^{g \delta T_b}}{C_\ell^{gg}} \quad (\text{B5})$$

which is again quite subdominant to $C_\ell^{T_\gamma T_\gamma}$.

Using the equality

$$\begin{aligned} \sigma_{C_\ell^{XY}}^2 &= \langle a_{\ell m}^X a_{\ell m}^{Y*} a_{\ell m}^{X*} a_{\ell m}^Y \rangle - (C_\ell^{XY})^2, \\ \sigma_{C_\ell^{XY} C_\ell^{XZ}} &= \langle a_{\ell m}^X a_{\ell m}^{Y*} a_{\ell m}^{X*} a_{\ell m}^Z \rangle - C_\ell^{XY} C_\ell^{XZ}, \end{aligned} \quad (\text{B6})$$

together with Eqs. (B2 – B6), we obtain

$$\begin{aligned} \sigma_{C_\ell^{g T_\gamma}}^2 &= (C_\ell^{g T_\gamma})^2 + C_\ell^{gg} C_\ell^{T_\gamma T_\gamma}, \\ \sigma_{C_\ell^{g T}}^2 &= (C_\ell^{g T})^2 + C_\ell^{gg} C_\ell^{TT} = \left(1 + \frac{\delta T_{21}}{T_{\gamma,0}}\right)^2 (C_\ell^{g T_\gamma})^2 + C_\ell^{gg} (C_\ell^{T_\gamma T_\gamma} + C_\ell^{\delta T_b \delta T_b}) \\ \sigma_{C_\ell^{g T_\gamma} C_\ell^{g T}} &= C_\ell^{g T_\gamma} C_\ell^{g T} + C_\ell^{gg} C_\ell^{T_\gamma T} = \left(1 + \frac{\delta T_{21}}{T_{\gamma,0}}\right) (C_\ell^{g T_\gamma})^2 + C_\ell^{gg} C_\ell^{T_\gamma T_\gamma}. \end{aligned} \quad (\text{B7})$$

Finally, using Eqs. (B1) and (B7) we obtain

$$\sigma_{s_\ell}^2(\bar{\nu}) = \langle T_{\gamma,0} \rangle^2 \frac{(C_\ell^{gg} + \bar{n}_g^{-1}) \left\{ C_\ell^{\delta T_b \delta T_b}(\bar{\nu}) + \epsilon_{\ell,T}(\bar{\nu}) + \left(\frac{\delta T_{21}(\bar{\nu})}{T_{\gamma,0}}\right)^2 C_\ell^{T_\gamma T_\gamma} \right\}}{(C_\ell^{g T_\gamma})^2 f_{\text{sky}}(2\ell + 1)}, \quad (\text{B8})$$

where systematic errors in auto-correlations are now included and the number of modes with imperfect sky coverage is accounted for as well. The net noise is given by

$$N^{-2}(\bar{\nu}) = \sum_{\ell=\ell_{\min}}^{\ell_{\max}} \sigma_{s_\ell}^{-2}(\bar{\nu}). \quad (\text{B9})$$

Fig. 1 shows how the observing time affects the SNR. In the case of $\Delta\nu = 5$ MHz, the gain from having $\Delta t = 30000$ hr instead of $\Delta t = 10000$ hr is not much, because the sky brightness noise is still too high at $z \sim 30$ and the lower-redshift ($z \lesssim 15 - 20$) noise is intrinsic, coming mostly from the 21-cm auto-correlation $C_\ell^{\delta T_b \delta T_b}(\bar{\nu})$. See the relative noise contribution in Fig. 5. The even easier $\Delta t = 3000$ hr case also gives moderate sensitivity during the early EoR phase, and thus should be considered seriously in the early run of the SKA1-LOW.

2. superstructure 21-cm ISW

If one were to use superstructures, this is not to use the power spectrum as the full-sky cross-correlation scheme does. Instead, this is close to the full imaging. Therefore, the automatic removal of the Milky Way foreground does not apply to this strategy. Let us imagine that we have the temperature field where all the foreground components (CMB, Milky Way, extragalactic) are removed.

The noise is estimated as follows. Superstructures are characterized by their large angular span, $\sim 4^\circ$ in radius, and the temperature field is convoluted with specific smoothing or matching filters $\psi^{\text{MF}}(|\hat{n} - \hat{n}_0|) = \psi^{\text{MF}}(\theta)$ where \hat{n}_0 is the location of the center of a superstructure and θ is the angle away from \hat{n}_0 . For example, [25] used a smoothing filter that averages the temperature in the region where $\theta < \theta_{\text{th}}$ and further subtracts the average temperature where $\theta_{\text{th}} < \theta < \sqrt{2}\theta_{\text{th}}$, and claimed the oddly strong ($A_{\text{ISW}} \simeq 5$) ISW effect on superstructures. We follow [28] to estimate the noise: we take three different matching filters shown in [28] that would each give the filtered 21-cm temperature field

$$\delta T_b'(\hat{n}', \bar{\nu}) = \int d\hat{n} \delta T_b(\hat{n}, \bar{\nu}) \psi^{\text{MF}}(|\hat{n}' - \hat{n}|). \quad (\text{B10})$$

The variance of this filtered field will be given by

$$\sigma_{\delta T_b}^2(\bar{\nu}) = \sum_{\ell} \left(C_\ell^{\delta T_b \delta T_b} + \epsilon_{\ell,T} \right) (\psi_{\ell 0}^{\text{MF}})^2, \quad (\text{B11})$$

which is synonymous to the mass variance of filtered density field, σ_M . Here, $\psi_{\ell 0}^{\text{MF}}$ is the expansion coefficient in Legendre polynomials of $\psi^{\text{MF}}(\theta)$:

$$\psi^{\text{MF}}(\theta) = \sum_{\ell} \psi_{\ell 0}^{\text{MF}} Y_{\ell 0}(\cos \theta). \quad (\text{B12})$$

We found that even with the difference in the three filters, the variance calculated by Eq. (B11) all lead to about the same values at all frequencies. We inverted Eq. (B12)

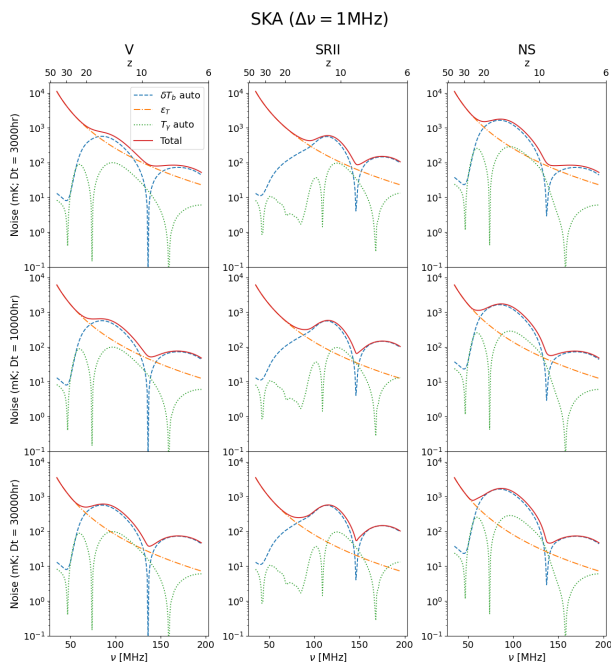


FIG. 5. Composition of the noise in the case of $\Delta\nu = 1$ MHz. Different observing times are also investigated (top: 3000 hr; middle: 10000 hr; bottom: 30000 hr). The sky brightness (ϵ_T : orange, dot-dashed) dominates the net noise (red, solid) at $z \gtrsim 15 - 20$, while the noise in the lower-redshift epoch is dominated by the uncontrollable, intrinsic quantity $C_\ell^{\delta T_b \delta T_b}$ (blue, dashed).

using orthogonality of $Y_{\ell 0}$, and calculated the integral to obtain $\psi_{\ell 0}^{\text{MF}}$ in a brute-force way. We took adaptively fine samples in the Legendre polynomials, which was somewhat computationally costly. Because $\psi_{\ell 0}^{\text{MF}}$ is a low- ℓ -pass filter, we obtained $\psi_{\ell 0}^{\text{MF}}$ only up to $\ell = 200$ and set the rest to zero. We found that $\psi_{\ell 0}^{\text{MF}}$ obtained this way reproduces $\psi^{\text{MF}}(\theta)$ well enough.

Because multiple superstructure ISW signals are stacked, if there are N_{ss} superstructures stacked then the final noise is given by

$$\sigma_{\delta T_b}^2(\bar{\nu}) = \sum_{\ell} \left(C_\ell^{\delta T_b \delta T_b} + \epsilon_{\ell, T} \right) (\psi_{\ell 0}^{\text{MF}})^2 / N_{\text{ss}}, \quad (\text{B13})$$

and the signal is given by Eq. (17) of the main text. We used Eq. (B13) to calculate the noise with $N_{\text{ss}} = 200$, twice as large as what was used in [25] or about 1/2 of that in [26], and obtained Fig. 3 of the main text.

-
- [1] R. K. Sachs and A. M. Wolfe, *Astrophys. J.* **147**, 73 (1967), *Perturbations of a cosmological model and angular variations of the microwave background*.
- [2] P. Fosalba, E. Gaztañaga, and F. J. Castander, *Astrophys. J. Lett.* **597**, L89 (2003), *Detection of the integrated sachs-wolfe and sunyaev-zeldovich effects from the cosmic microwave background-galaxy correlation*.
- [3] N. Afshordi, Y.-S. Loh, and M. A. Strauss, *Phys. Rev. D* **69**, 083524 (2004), *Cross-correlation of the cosmic microwave background with the 2mass galaxy survey: Signatures of dark energy, hot gas, and point sources*.
- [4] A. Cabré, E. Gaztañaga, M. Manera, P. Fosalba, and F. Castander, *Mon. Not. Roy. Astron. Soc.* **372**, L23 (2006), *Cross-correlation of wilkinson microwave anisotropy probe third-year data and the sloan digital sky survey dr4 galaxy survey: new evidence for dark energy*.
- [5] T. Giannantonio and R. Crittenden, *Mon. Not. Roy. Astron. Soc.* **381**, 819 (2007), *The effect of reionization on the cosmic microwave background-density correlation*.
- [6] S. Ilić, M. Douspis, M. Langer, A. Pénin, and G. Lagache, *Mon. Not. Roy. Astron. Soc.* **416**, 2688 (2011), *Cross-correlation between the cosmic microwave and infrared backgrounds for integrated sachs-wolfe detection*.
- [7] T. Giannantonio, R. Crittenden, R. Nichol, and A. J. Ross, *Mon. Not. Roy. Astron. Soc.* **426**, 2581 (2012), *The significance of the integrated sachs-wolfe effect revisited*.
- [8] Planck Collaboration, P. A. R. Ade, N. Aghanim, M. Arnaud, M. Ashdown, J. Aumont, C. Baccigalupi, A. J. Banday, R. B. Barreiro, N. Bartolo, et al., *A&A* **594**, A21 (2016), *Planck 2015 results. xxi. the integrated sachs-wolfe effect*.
- [9] F. Dong, Y. Yu, J. Zhang, X. Yang, and P. Zhang, *Mon. Not. Roy. Astron. Soc.* **500**, 3838 (2021), *Measuring the integrated sachs-wolfe effect from the low-density regions of the universe*.
- [10] B. Bahr-Kalus, D. Parkinson, J. Asorey, S. Camera, C. Hale, and F. Qin, *Mon. Not. Roy. Astron. Soc.* **517**, 3785 (2022), *A measurement of the integrated sachs-wolfe effect with the rapid askap continuum survey*.
- [11] R. G. Crittenden and N. Turok, *Phys. Rev. Lett.* **76**, 575 (1996), *Looking for a cosmological constant with the rees-sciamia effect*.
- [12] M. Kamionkowski, *Phys. Rev. D* **54**, 4169 (1996), *Matter-microwave correlations in an open universe*.
- [13] Y.-S. Song, W. Hu, and I. Sawicki, *Phys. Rev. D* **75**, 044004 (2007), *Large scale structure of $f(r)$ gravity*.
- [14] Y.-C. Cai, B. Li, S. Cole, C. S. Frenk, and M. Neyrinck, *Mon. Not. Roy. Astron. Soc.* **439**, 2978 (2014), *The integrated sachs-wolfe effect in $f(r)$ gravity*.
- [15] J. D. Bowman, A. E. E. Rogers, R. A. Monsalve, T. J. Mozdzen, and N. Mahesh, *Nature (London)* **555**, 67 (2018), *An absorption profile centred at 78 megahertz in the sky-averaged spectrum*.
- [16] S. Singh, N. T. Jishnu, R. Subrahmanyam, N. Udaya

- Shankar, B. S. Girish, A. Raghunathan, R. Somashekar, K. S. Srivani, and M. Sathyanarayana Rao, *Nature Astronomy* **6**, 607 (2022), *On the detection of a cosmic dawn signal in the radio background.*
- [17] R. Barkana, *Nature (London)* **555**, 71 (2018), *Possible interaction between baryons and dark-matter particles revealed by the first stars.*
- [18] R. Hills, G. Kulkarni, P. D. Meerburg, and E. Puchwein, *Nature (London)* **564**, E32 (2018), *Concerns about modelling of the edges data.*
- [19] A. Raccanelli, E. Kovetz, L. Dai, and M. Kamionkowski, *Phys. Rev. D* **93**, 083512 (2016), *Detecting the integrated sachs-wolfe effect with high-redshift 21-cm surveys.*
- [20] S. C. Hotinli and K. Ahn, arXiv e-prints arXiv:2305.01672 (2023), *Probing the global 21-cm background by velocity-induced dipole and quadrupole anisotropies.*
- [21] N. Afshordi, *Phys. Rev. D* **70**, 083536 (2004), *Integrated sachs-wolfe effect in cross-correlation: The observer's manual.*
- [22] M. Zaldarriaga, S. R. Furlanetto, and L. Hernquist, *Astrophys. J.* **608**, 622 (2004), *21 Centimeter Fluctuations from Cosmic Gas at High Redshifts.*
- [23] D. J. Fixsen, E. S. Cheng, J. M. Gales, J. C. Mather, R. A. Shafer, and E. L. Wright, *Astrophys. J.* **473**, 576 (1996), *The Cosmic Microwave Background spectrum from the full COBE FIRAS data set.*
- [24] D. J. Fixsen, *Astrophys. J.* **707**, 916 (2009), *The temperature of the cosmic microwave background.*
- [25] B. R. Granett, M. C. Neyrinck, and I. Szapudi, *Astrophys. J. Lett.* **683**, L99 (2008), *An imprint of superstructures on the microwave background due to the integrated sachs-wolfe effect.*
- [26] S. Nadathur, S. Hotchkiss, and S. Sarkar, *J. Cosmol. Astropart. Phys.* **2012**, 042 (2012), *The integrated sachs-wolfe imprint of cosmic superstructures: a problem for Λ cdm.*
- [27] S. Flender, S. Hotchkiss, and S. Nadathur, *J. Cosmol. Astropart. Phys.* **2013**, 013 (2013), *The stacked isw signal of rare superstructures in Λ cdm.*
- [28] S. Nadathur and R. Crittenden, *Astrophys. J. Lett.* **830**, L19 (2016), *A detection of the integrated sachs-wolfe imprint of cosmic superstructures using a matched-filter approach.*
- [29] A. Kovács, C. Sánchez, J. García-Bellido, J. Elvin-Poole, N. Hamaus, V. Miranda, S. Nadathur, T. Abbott, F. B. Abdalla, J. Annis, et al., *Mon. Not. Roy. Astron. Soc.* **484**, 5267 (2019), *More out of less: an excess integrated sachs-wolfe signal from supervoids mapped out by the dark energy survey.*
- [30] Q. Hang, S. Alam, Y.-C. Cai, and J. A. Peacock, *Mon. Not. Roy. Astron. Soc.* **507**, 510 (2021), *Stacked cmb lensing and isw signals around superstructures in the desi legacy survey.*
- [31] A. Kovács, R. Beck, A. Smith, G. Rácz, I. Csabai, and I. Szapudi, *Mon. Not. Roy. Astron. Soc.* **513**, 15 (2022), *Evidence for a high-z isw signal from supervoids in the distribution of eboss quasars.*
- [32] S. R. Furlanetto, *Mon. Not. Roy. Astron. Soc.* **371**, 867 (2006), *The global 21-centimeter background from high redshifts.*
- [33] K. Ahn, I. T. Iliev, P. R. Shapiro, G. Mellema, J. Koda, and Y. Mao, *Astrophys. J. Lett.* **756**, L16 (2012), *Detecting the Rise and Fall of the First Stars by Their Impact on Cosmic Reionization.*
- [34] K. Ahn and P. R. Shapiro, *Astrophys. J.* **914**, 44 (2021), *Cosmic Reionization May Still Have Started Early and Ended Late: Confronting Early Onset with Cosmic Microwave Background Anisotropy and 21 cm Global Signals.*
- [35] C. M. Trott, C. H. Jordan, S. Midgley, N. Barry, B. Greig, B. Pindor, J. H. Cook, G. Sleap, S. J. Tingay, D. Ung, et al., *Mon. Not. Roy. Astron. Soc.* **493**, 4711 (2020), *Deep multiredshift limits on epoch of reionization 21 cm power spectra from four seasons of murchison widefield array observations.*
- [36] R. Ghara, S. K. Giri, G. Mellema, B. Ciardi, S. Zaroubi, I. T. Iliev, L. V. E. Koopmans, E. Chapman, S. Gazagnes, B. K. Gehlot, et al., *Mon. Not. Roy. Astron. Soc.* **493**, 4728 (2020), *Constraining the intergalactic medium at $z \sim 9.1$ using lofar epoch of reionization observations.*
- [37] HERA Collaboration, Z. Abdurashidova, T. Adams, J. E. Aguirre, P. Alexander, Z. S. Ali, R. Baartman, Y. Balfour, R. Barkana, A. P. Beardsley, et al., *Astrophys. J.* **945**, 124 (2023), *Improved constraints on the 21 cm eor power spectrum and the x-ray heating of the igm with hera phase i observations.*
- [38] L. Yan, E. Donoso, C.-W. Tsai, D. Stern, R. J. Assef, P. Eisenhardt, A. W. Blain, R. Cutri, T. Jarrett, S. A. Stanford, et al., *Astron. J.* **145**, 55 (2013), *Characterizing the mid-infrared extragalactic sky with wise and sdss.*
- [39] O. Doré, J. Bock, M. Ashby, P. Capak, A. Cooray, R. de Putter, T. Eifler, N. Flagey, Y. Gong, S. Habib, et al., arXiv e-prints arXiv:1412.4872 (2014), *Cosmology with the spherex all-sky spectral survey.*
- [40] A. A. Deshpande, *Astrophys. J. Lett.* **866**, L7 (2018), *Dipole anisotropy as an essential qualifier for the monopole component of the cosmic-dawn spectral signature, and the potential of diurnal pattern for foreground estimation.*
- [41] L. Koopmans, J. Pritchard, G. Mellema, J. Aguirre, K. Ahn, R. Barkana, I. van Bemmel, G. Bernardi, A. Bonaldi, F. Briggs, et al., in *Advancing Astrophysics with the Square Kilometre Array (AASKA14)* (2015), p. 1, 1505.07568.
- [42] A. Lewis and A. Challinor, *Camb: Code for anisotropies in the microwave background*, Astrophysics Source Code Library, record ascl:1102.026 (2011), 1102.026, URL <https://ui.adsabs.harvard.edu/abs/2011ascl.soft02026L>.
- [43] R. Barkana and A. Loeb, *Astrophys. J. Lett.* **624**, L65 (2005), *A Method for Separating the Physics from the Astrophysics of High-Redshift 21 Centimeter Fluctuations.*
- [44] X. Fang, E. Krause, T. Eifler, and N. MacCrann, *J. Cosmol. Astropart. Phys.* **2020**, 010 (2020), *Beyond limber: efficient computation of angular power spectra for galaxy clustering and weak lensing.*
- [45] A. Cabré, P. Fosalba, E. Gaztañaga, and M. Manera, *Mon. Not. Roy. Astron. Soc.* **381**, 1347 (2007), *Error analysis in cross-correlation of sky maps: application to the integrated sachs-wolfe detection.*
- [46] T. Giannantonio, R. Scranton, R. G. Crittenden, R. C. Nichol, S. P. Boughn, A. D. Myers, and G. T. Richards, *Phys. Rev. D* **77**, 123520 (2008), *Combined analysis of the integrated sachs-wolfe effect and cosmological implications.*
- [47] M. A. Alvarez, E. Komatsu, O. Doré, and P. R. Shapiro,

Astrophys. J. **647**, 840 (2006), *The cosmic reionization history as revealed by the cosmic microwave background*

doppler-21 cm correlation.